Suppression of geometric frustration by magnetoelastic coupling in AuCrS$_2$

S. J. E. Carlsson,[1,2,*] G. Rousse,[1] I. Yamada,[1,3] H. Kuriki,[3] R. Takahashi,[3] F. Lévy-Bertrand,[2] G. Giriat,[4] and A. Gauzzi[1]

[1]*Institut de Minéralogie et de Physique des Milieux Condensés, Université Pierre et Marie Curie,*
Sorbonne Universités and CNRS, 75005 Paris, France
[2]*Institut Néel, CNRS and Université Joseph Fourier, BP166, 38042 Grenoble, France*
[3]*Department of Chemistry, Graduate School of Science and Engineering, Ehime University, Matsuyama, Ehime 790-8577, Japan*
[4]*Centre for Science at Extreme Conditions and School of Engineering, University of Edinburgh, Edinburgh EH9 3JZ, United Kingdom*

We studied the structural, magnetic, and electronic properties of the geometrically frustrated layered AuCrS$_2$ system by means of x-ray and neutron powder diffraction, specific heat, dc magnetization, and dc electrical resistivity measurements. The room-temperature structural refinement is consistent with a hexagonal centrosymmetric R-$3m$ symmetry and with formal valence states Au$^+$ and Cr^{3+}, where the Cr^{3+} ions form a regular triangular lattice within the hexagonal planes. On cooling, we observe a first-order structural phase transition to a monoclinic $C2/m$ symmetry concomitant to an antiferromagnetic order at T_N = 47 K. The atomic displacements associated with this transition stretch the triangular lattice, thus suppressing the geometric frustration. This accounts for the magnetic order observed and gives evidence of a large magnetoelastic coupling. The refined magnetic structure is commensurate and consists of double ferromagnetic chains along the stretching direction with $\mu = 2.54\ \mu_B/$Cr^{3+}; the residual frustration stabilizes an elegant pattern of alternate ferromagnetic and antiferromagnetic intra- and interplane couplings between adjacent chains. The electrical transport of our sintered powder samples is found to be semiconducting-like with $\rho_{300K} \sim 157\ \Omega$cm and an activation energy of 0.38 eV.

I. INTRODUCTION

During the last decades, the physics of spin frustration in triangular lattice antiferromagnets (TLA) has attracted a great deal of interest due to the interplay between lattice geometry and electronic properties.[1,2] In case the lattice and electronic degrees of freedom are coupled, the frustration can be suppressed by distorting the triangular lattice. In layered compounds, this coupling leads to a rich manifold of three-dimensional orderings that depend on the stacking of the layers and on the anisotropy. Recently, incommensurate spin structures and improper ferroelectricity have been reported.[3–5] Delafossite-like compounds ABO$_2$ offer an interesting playground for studying these orderings thanks to the simple structure where the B ions form a triangular lattice within the BO$_2$ layers, and the latter are linked by the A ion. If the B ion is magnetic, geometric frustration is then achieved, as the dominant intraplane interaction is antiferromagnetic (AFM). In the chromium system ACrO$_2$ (A = Ag, Cu, Pd, and Na), the most common spin ordering observed at low temperature is the 120° spiral structure with weak interplane coupling. This type of structure, common for TLA systems in general,[6–9] has been found to induce ferroelectricity in AgCrO$_2$ and CuCrO$_2$ (Refs. 10 and 11), which is promising for the design of multiferroic materials.

The sulfide counterparts ACrS$_2$ (A = Ag, Cu, Na, Li, and K)[12–16] of the above oxides share with the latter a similar structure with triangular Cr layers. All compounds are found to order AFM at low temperatures. However, the orderings are very different from one another. They range from an incommensurate helical structure in NaCrS$_2$ (Ref. 12) and CuCrS$_2$ (Ref. 15) to the 120° spin structure in LiCrS$_2$ (Ref. 16) and the commensurate structures in KCrS$_2$ (Ref. 12) and AgCrS$_2$.[17] A recent work has reported that the latter compound

is a multiferroic,[18] where ferroelectricity is driven by the AFM order, similarly to the case of AgCrO$_2$ and CuCrO$_2$. It turns out that the magnetoelectric coupling in AgCrS$_2$ is concomitant to large magnetoelastic effects previously reported in NaCrS$_2$ (Ref. 19) and CuCrS$_2$ (Ref. 15), but not in their oxide counterparts. This difference may be due to a comparatively small contribution of the electrostatic energy to the total energy, a consequence of the reduced ionicity of sulfides as compared to oxides. In geometrically frustrated systems, this situation may lead to a large magnetoelastic response, for the magnetic ordering requires a significant distortion of the lattice.

In light of the above considerations, the study of magnetic frustration in sulfides with geometric frustration may provide new hints for the effective design of multiferroic materials. In order to address this point, in this paper, we have studied the correlation between the structural distortions and the magnetic properties in AuCrS$_2$. A previous study has shown that, at room temperature, AuCrS$_2$ crystallizes in the hexagonal space group $R3m$ and becomes AFM below the Néel temperature (T_N) of 55 K.[20] It exhibits a layered structure with a triangular lattice of Cr^{3+} ions similar to that of other ACrS$_2$ compounds. However, the stacking sequence of the CrS$_2$ layers is different, as the Au atoms are linearly coordinated with two S atoms of adjacent layers. In light of this, AuCrS$_2$ is a candidate for unusual orderings and possibly multiferroicity. No low temperature studies of the crystal and magnetic structure of AuCrS$_2$ have previously been made. Therefore, we have performed neutron and synchrotron x-ray powder diffraction and physical properties measurements between room temperature and 2 K. First, we have redetermined the room temperature nuclear structure. Our data suggest a centrosymmetric R-$3m$ space group, contrary to the $R3m$

one reported previously. Second, we found that the AFM ordering at 47 K (slightly lower than previously reported) is accompanied by a structural transition to a monoclinic phase. The large atomic displacements associated with this transition give evidence of a large magnetoelastic coupling and account for the stability of the above magnetic ordering. Our structural study enabled us to fully determine the magnetic structure. In the latter, the moments in the Cr^{3+} planes order in a collinear and commensurate four-sublattice structure, characterized by an up-up-down-down arrangement of the spins. We show that both second- and third-nearest neighbor interactions between Cr^{3+} ions must be taken into account to explain the stabilization of this unusual magnetic order, as reported for other compounds presenting superexchange interactions.[21–24]

II. EXPERIMENTAL DETAILS

Polycrystalline $AuCrS_2$ samples were prepared by a standard solid state reaction method following Fukuoka *et al.*[20] In brief, stoichiometric amounts of Au powder (Aldrich, 99.99%), Cr powder (Aldrich, 99%) and S powder (Sigma, 99.98%) were ground in an agate mortar and pressed into pellets. The pellets were sealed in evacuated silica tubes and heated in a furnace at 1000 °C for 48 h. A structural characterization of the $AuCrS_2$ sample was carried out at 300 K by using a laboratory powder x-ray diffraction equipped with a Co K_α source ($\lambda = 1.7890$ Å), and no impurity phases were detected.

Neutron diffraction patterns were recorded as a function of temperature in the 2–300 K range using the constant wavelength instrument Super-D2B at the Institut Laue-Langevin in Grenoble, France. This instrument features a bank of 128 collimated, linear-wire, position-sensitive detectors separated by 1.25°, stepped in 0.05 intervals. The sample was contained in a vanadium can, and data were collected in the angular range $10° \leqslant 2\theta \leqslant 150°$ at a wavelength of $\lambda = 1.594$ Å. Rietveld[25] refinements of the structural models were performed with the General Structure Analysis System (GSAS)[26] and FullProf[27] suite of programs. Complementary synchrotron x-ray diffractograms were taken at room temperature at a wavelength of 0.52310 Å at the BL02B2 beamline of SPring-8 facility in Japan.[28]

Magnetic susceptibility measurements were carried out on a commercial Quantum Design Magnetic Property Measurement System (MPMS) magnetometer in the 4–300 K range with an applied external field of 5 kOe. The electrical resistivity was measured as a function of temperature using a four-point contact method on a bar-shaped sample of $\sim 1 \times 2 \times 4$ mm^3 on a commercial Quantum Design Physical Property Measurement System (PPMS). Specific heat measurements were also performed using a semi-adiabatic relaxation technique implemented in the PPMS. Where the heat capacity was almost constant over the spanned temperatures response (outside the transition region), both the heating and cooling branches at each point were fitted at the same time using a standard 2τ-model[29] and a single value of specific heat extracted. In the transition region, a slope analysis of the time-dependent temperature response, suitable to study to first-order phase transitions, was used to extract the changes of the specific heat upon both heating and cooling.

III. RESULTS

A. Room temperature nuclear structure

In a previous report by Fukuoka *et al.*,[20] the room temperature structure of $AuCrS_2$ was refined in both the hexagonal noncentrosymmetric $R3m$ and the centrosymmetric R-$3m$ space groups. The authors found that the two structural models yielded equivalent results for the atomic parameters (Table I). However, the latter refinement resulted in higher residuals, and the anisotropic thermal parameters for the S atom did not converge on realistic values, hence the $R3m$ space group was proposed. In this paper, we have reexamined this point by carrying out a Rietveld refinement of powder diffraction data collected at room temperature by using three different laboratory x-ray, high-resolution neutron, and synchrotron x-ray diffractometers. The results of the refinement of the former data are summarized in Table I. One notes that, contrary to the above report, the quality of our refinement is equivalent or slightly better in the R-$3m$ symmetry. Furthermore, in the $R3m$ symmetry, the z parameters of the S and Au atoms do not converge. A comparison between experimental and calculated profiles in the R-$3m$ symmetry is shown in Fig. 1(a), which shows the good quality of the structural refinement. Similar results were obtained by refining the neutron powder diffraction data (see Table II) and the synchrotron data (not shown). In conclusion, our refinement clearly suggests that the higher symmetry R-$3m$ space group should be preferred to describe the room-temperature nuclear structure of $AuCrS_2$. The

TABLE I. Rietveld refinement results of x-ray diffraction data of $AuCrS_2$ at 300 K, using the space groups $R3m$ and R-$3m$. In the former case, the atomic coordinates, z, along the c axis are not set by symmetry, thus the z value of Cr was fixed to 0. Values taken from the literature have also been added for comparison. Atomic positions for the $R3m$ symmetry are Au, $(0, 0, z)$, Cr, $(0, 0, z)$, S, $(0, 0, z)$ and for R-$3m$ Au, $(0, 0, 1/2)$, Cr, $(0, 0, 0)$, S, $(0, 0, z)$.

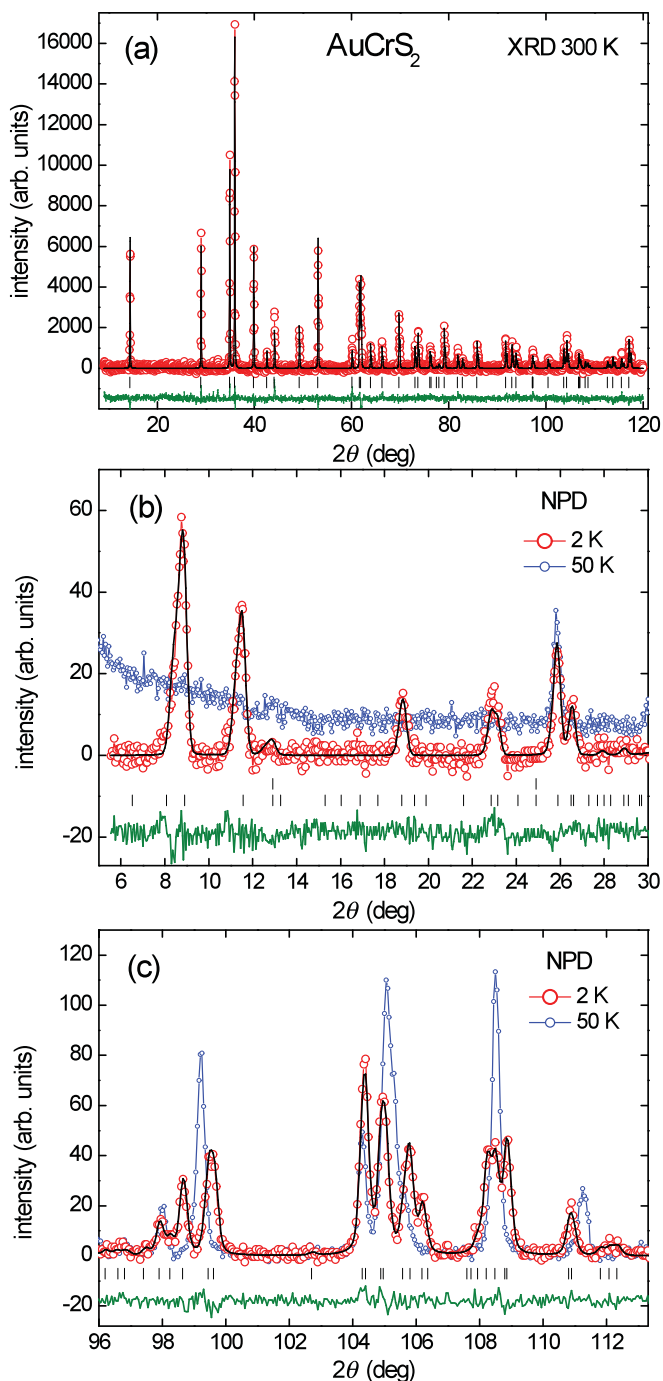| Refined parameters	$R3m$ Lit. (Ref. 20)	R-$3m$ Lit. (Ref. 20)	$R3m$ (our study)	R-$3m$ (our study)
a (Å)	3.4823(4)	3.4823(4)	3.48200(4)	3.48206(4)
c (Å)	21.463(3)	21.463(3)	21.4582(4)	21.4586(3)
Au z	0.4994(14)	0.5	0.498(3)	0.5
Cr z	0	0	0	0
S z	0.607(3),0.392(2)	0.610(3)	0.606(4),0.387(5)	0.6084(4)
wR_p, R_p (%)	5.39,4.76	10.76,8.65	1.93,1.45	1.90,1.45

FIG. 1. (Color online) Observed (red circles), calculated (black), and difference (green) patterns from the Rietveld analysis of x-ray and neutron powder diffraction data for $AuCrS_2$. (a) Fit to the XRD pattern collected at 300 K and $\lambda = 1.7890$ Å. (b) Low- and (c) high-angle region of the NPD data collected at 2 K (refined) and 50 K (raw data) illustrating the magnetic reflections which disappear at 50 K and the splitting of the nuclear Bragg peaks below T_N.

lattice parameters obtained from the refinement of the neutron diffraction pattern are as follows: $a_h = b_h = 3.4826(1)$ Å and $c_h = 21.4622(8)$ Å, in good agreement with our x-ray diffraction data and the previous report by Fukuoka *et al.*[20]

The room-temperature nuclear structure of $AuCrS_2$ is shown in Fig. 2(a). Note the linear (dumbbell) coordination

TABLE II. Structural parameters for $AuCrS_2$ from the Rietveld refinements to 300 and 2 K high-resolution neutron powder diffraction data. Atomic positions for the R-$3m$ symmetry are for Au $3b$ (0, 0, $\frac{1}{2}$), Cr $3a$ (0, 0, 0), and S $6c$ (0, 0, z) and for the $C2/m$ symmetry Au $2d$ (0, $\frac{1}{2}$, $\frac{1}{2}$), Cr $3a$ (0, 0, 0), and S $4i$ (x, 0, z).

	Temperature and space group	
Refined parameter	300 K, R-$3m$	2 K, $C2/m$
a (Å)	3.4826(1)	14.4478(5)
b (Å)		3.4976(1)
c (Å)	21.4622(8)	7.4197(3)
β (°)		156.454(1)
V (Å^3)	225.43(1)	149.777(5)
S x		0.6056(6)
S z	0.6068(1)	0.389(1)
R_P, wR_P, R_{F2} (%)	5.20, 6.66, 8.15	5.12, 6.62, 10.33

of the Au ion connecting two adjacent S layers along the c axis. We recall that the same structure is adopted by $CuFeO_2$ (Ref. [30]) and $ACrO_2$ ($A =$ Cu, Ag),[10,31] whilst in the sulfide counterparts $ACrS_2$ ($A =$ Cu, Ag), the A^+ ion is tetrahedrally coordinated.[12] As a result, the coordination of the Cr atom is octahedral in $AuCrS_2$ with six equal Cr-S distances and trigonal prismatic in $CuCrS_2$ and in $AgCrS_2$. This leads to two different stacking sequences of the sulfur atom along the c axis. The sequence is of the AB-BC-CA type in $AuCrS_2$ and of the CB-AC-BA one in $CuCrS_2$ and in $AgCrS_2$ [Fig. 2(b)]. A third type of structure with trigonal prismatic coordination of the metal atom and a linear coordination of the A cation was reported in $AuVS_2$ which displays semimetallic properties.[32]

As mentioned previously, in the above high-temperature hexagonal structure, the Cr atoms form a triangular lattice in the hexagonal plane with a Cr-Cr distance of 3.4826(1) Å, very similar to the case of $CuCrS_2$. The interatomic distances suggest formal valence states of Au$^+$ and Cr^{3+}, although it is known that an ionic model is less suited for sulfides than for oxides.
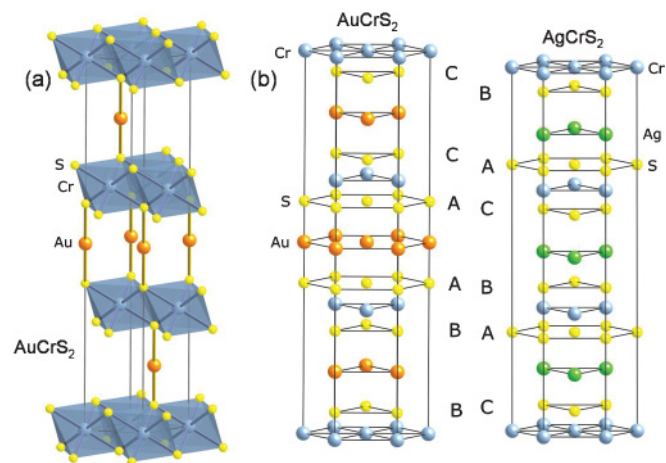

FIG. 2. (Color online) (a) The R-$3m$ crystal structure of $AuCrS_2$. (b) The stacking patterns of sulfur atoms along the c axis in $AuCrS_2$ and $AgCrS_2$.
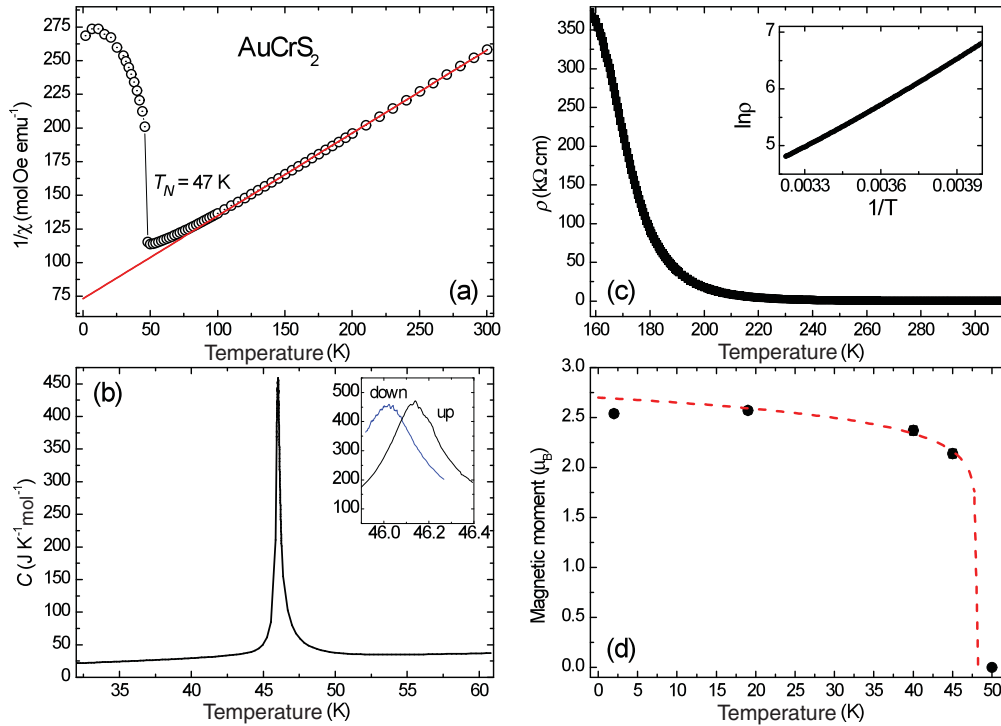
FIG. 3. (Color online) (a) Temperature dependence of the inverse magnetic susceptibility (χ^{-1}) of AuCrS$_2$ measured at a field of $H = 5000$ Oe. An antiferromagnetic anomaly is clearly visible at $T_N = 47$ K. The solid line (red) represents the linear Curie–Weiss fit to the high-temperature part of the curve. (b) Specific heat (C) measured on cooling. The inset shows the hysteresis observed between cooling and heating. (c) Electrical resistivity (ρ). The inset shows the inverse temperature dependence of the high-temperature resistivity values. (d) The magnetic moment refined against the neutron powder diffraction data. A power law [$m(T) = A(1 - T/T_N)^\beta$] curve (red dashed line) is shown as a guide to the eye.

B. Specific heat, magnetic susceptibility, and electrical transport

In Fig. 3(a), we report the inverse magnetic susceptibility $\chi^{-1}(T)$ curve as a function of temperature, T, in the 2–300 K range. The data confirm the previous observation[20] of AFM transition at $T_N = 47(1)$ K, although this Néel temperature is somehow lower than that of $\sim$55 K previously reported. A Curie–Weiss fit of the linear part of the curve yields a Weiss temperature $\Theta_W = -119.0(7)$ K and an effective paramagnetic moment $\mu_{eff} = 3.61(1)\mu_B$/Cr. The latter value is close to the spin-only value $\mu_{3/2} = 3.87\mu_B$ expected for a free Cr^{3+} ion in the high-spin state $S = 3/2$, similarly to the case of CuCrS$_2$ and AgCrS$_2$.[15,18] Upward deviations from the Curie–Weiss law were observed below 125 K, which is attributed to antiferromagnetic fluctuations. An indication of the degree of frustration is provided by the ratio $|\Theta_W|/T_N$ which is 2.48 for AuCrS$_2$, comparable to the values reported for CuCrS$_2$ and AgCrS$_2$.[15,17] This is a rather small value, suggesting a modest frustration as compared to the case of strongly frustrated systems, which typically exhibit values larger than 10.[33]

Figure 3(b) shows the temperature dependence of the specific heat, $C(T)$, measured on our powder samples of AuCrS$_2$. The sharp jump at the AFM transition confirms the occurrence of a phase transition. In addition, the small though significant hysteresis of 0.13(2) K observed upon cooling and warming is indicative of a first-order transition, in agreement with the diffraction data. The transition point extracted from the specific heat data is $T_N = 46.3(5)$ K, in good agreement with the mag-

netic susceptibility data. The amplitude of the hysteresis and the maximum value of the specific heat were confirmed by repeating the pulse measurements with different amounts of heat.

The electrical resistivity shown in Fig. 3(c) reveals semiconducting behavior with a room-temperature resistivity $\rho_{300K} \sim 157$ Ωcm, slightly larger than the value reported for CuCrS$_2$ (20 Ωcm) but much smaller than that of AgCrS$_2$ ($>2 \times 10^7$ Ωcm).[18] Below 200 K, the resistivity rapidly increases and reaches 3.5×10^5 Ωcm at 150 K. This value corresponds to the maximum value of resistance that can be measured using our apparatus. Hence, we could not investigate the low-temperature behavior to verify whether the charge transport is affected by the magnetic ordering at 47 K. Comparably high resistivity values were reported in CuCrO$_2$, where ρ exceeds 10^5 Ωcm below 200 K and $\rho_{300K} \sim 10^3$ Ωcm.[34]

At high temperatures, the resistivity of AuCrS$_2$ follows a thermally activated behavior $\ln \rho \propto \Delta/T$ typical for a semiconductor [see inset of Fig. 3(c)]. Our data fit yields an activation energy $\Delta = 0.38$ eV. Also, this value is comparable to that reported in CuCrO$_2$ (0.28eV),[29] which confirms the similarity between the two compounds. We account for the insulating properties of both compounds by invoking a model of predominant super exchange interaction between the t_{2g} electrons of the Cr^{3+} ions, consistent with the AFM ordering.

C. Low-temperature nuclear and magnetic structure

Figure 1(b) gives the details of the low-angle (2θ) region of the neutron powder diffraction patterns collected just above

TABLE III. Selected interatomic distances and angles in $AuCrS_2$ at 300 and 2 K from the Rietveld refinements of Table II. NN refers to nearest neighbor and NNN to next-nearest neighbor.

	Temperature	
Distance/angle	300 K	2 K
Au-S1	2.293(2)Å $\times$ 2	2.3013(2)Å $\times$ 2
Cr-S1	2.386(1)Å $\times$ 6	2.3804(3)Å $\times$ 2
Cr-S2		2.3793(2)Å $\times$ 4
Cr-Cr (NN)	3.4826(1)Å $\times$ 6	3.4976(1)Å $\times$ 2
		3.4671(5)Å $\times$ 4
Cr-Cr (NNN)	6.032(5)Å $\times$ 6	5.988(5)Å $\times$ 2
		6.040(5)Å $\times$ 4
CrS_2 layer	2.569(5)Å	2.553(5)Å
Cr-S-Cr	93.67(7)°	93.563(5)°
		94.658(9)°
S-Cr-S	86.33(7)°	85.342(9)°
		86.437(5)°

(50 K) and below (2 K) the AFM transition. One notes the appearance of several prominent magnetic Bragg peaks below 45 K, in accordance with the evidence of an AFM ordering at $T_N \sim 47$ K given by the susceptibility data. This observation is concomitant to a splitting of the nuclear Bragg peaks at the same temperature, which is seen in the high-angle region of Fig. 1(c). This put into evidence a simultaneous antiferromagnetic and structural phase transition to a lower symmetry. In order to determine the nuclear and magnetic structures at low temperature, we consider that the isostructural compound $CuFeO_2$ undergoes a symmetry lowering structural phase transition at T_N from a hexagonal R-$3m$ to a monoclinic $C2/m$ structure.[30] A straightforward analysis shows that the same low-symmetry $C2/m$ space group also accounts for our diffraction patterns [Fig. 1(c)]. $C2/m$ is a subgroup of R-$3m$, and the Landau expansion describing the symmetry lowering contains a third-order invariant.[35] Therefore, according to Landau theory,[36] a first-order transition is expected, in accordance with the specific heat data. The lattice constants of the low-temperature $C2/m$ phase were determined to be $a_m = 14.4478(5)$ Å, $b_m = 3.4976(1)$ Å, and $c_m = 7.4197(3)$ Å, and $\beta = 156.454(1)°$. The refined structural parameters obtained using the D2B data at 300 and 2 K are reported in Tables II and III, while the two unit cells are schematically represented in Fig. 4(a). From this figure, one notes that the monoclinic distortion is driven by a shear distortion in the ab plane described by the β angle.

A further insight into the structural distortions associated with the phase transition can be gained by analyzing the temperature dependence of the structural parameters in Figs. 5(a)–5(d). In Figs. 5(a)–5(b), one notes that, above the transition, the unit cell parameters of the hexagonal structure, a_h, c_h, and the unit cell volume V_h all decrease upon cooling. A sharp drop to lower values is observed at T_N for c_h and V_h whereas a_h increases suddenly. Upon further cooling, all parameters including the monoclinic angle, β, increase. The symmetry-lowering is then caused by a stretching of the triangular Cr lattice along the a_h (or b_m) axis. As a result, the Cr-Cr distances and the Cr-S-Cr bond angles are enlarged along the b_m axis and slightly reduced in the two other
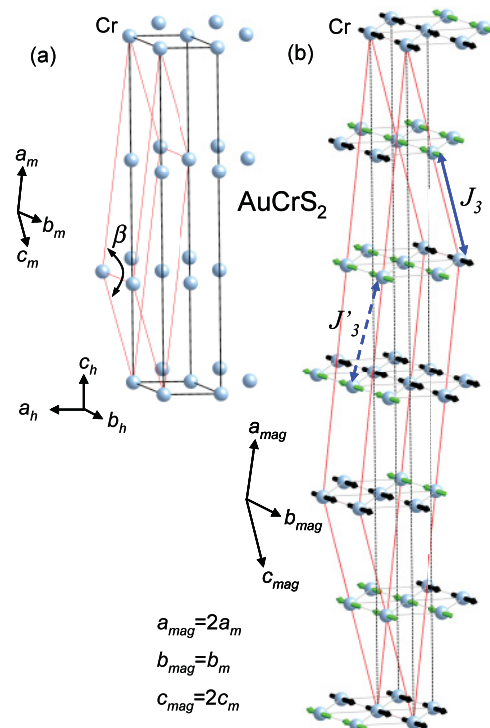

FIG. 4. (Color online) (a) Relation between the hexagonal (black lines) and the monoclinic (red lines) unit cells. (b) Illustration of the magnetic structure determined by neutron powder diffraction. The small arrows (green and black) correspond to the Cr^{3+} spin orientations and the two larger ones (blue) show the interplane interactions and the directions along which the up-up-down-down (dashed line) and antiferromagnetic (full line) configuration is found.

pseudohexagonal directions, forming an angle of $\pm120°$ with the b_m axis. These distortions lead to the formation of two long nearest neighbor (NN) Cr-Cr distances of 3.4976(1) Å and of four short distances of 3.4671(5) Å (see Fig. 6). They also lead to two inequivalent intraplanar next-nearest neighbor (NNN) distances of 5.988(5) Å and 6.040(5) Å perpendicular and 150° from the b_m direction, respectively. Below T_N, the larger Cr-Cr distance follows the same behavior as the interlayer shear described by the β angle. The contraction of the c axis means that the Au and Cr layers move closer together, but the Au-Cr distances remain almost unchanged due to the shear along the Cr layers. In the monoclinic phase, there are two distinct values of Cr-Cr interlayer distances [7.419(5) Å and 7.432(5) Å]. However, their difference is modest as compared to the degree of anisotropy of the Cr-Cr intralayer distances. The Cr-S distances become slightly smaller at the transition, hence the CrS_2 layer thickness is reduced [see Fig. 5(c)]. This is compensated by an increase of the Au-S bond length, which suggests an increased ionicity of the Au-S bond in the AFM phase. The temperature variation of the refined magnetic moment [Fig. 3(d)], the monoclinic angle, β, and b_m-axis length (Fig. 5) all follow the same critical behavior at the magnetic transition temperature. This confirms that the structural distortion and the magnetic ordering are correlated, which points at a large magnetoelastic coupling.
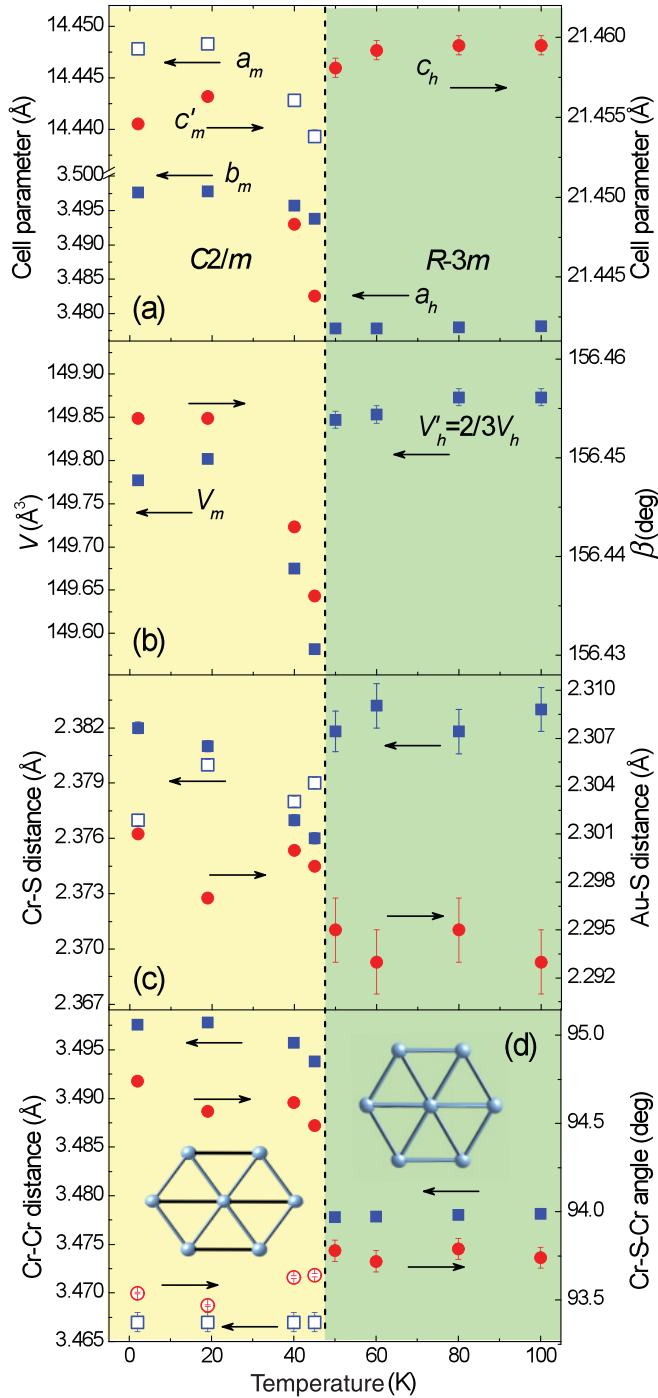
FIG. 5. (Color online) Temperature dependence of (a) lattice parameters a, b, and c, where c'_m is taken as the distance between two Cr ions three layers apart (equivalent to the c_h axis), (b) cell volume, where for comparison $V'_h = 2/3V_h$, and monoclinic angle, β, (c) Cr-S and Au-S bond lengths, and (d) Cr-Cr bond distance and Cr-S-Cr angle. Blue squares belong to the left y axis, while red circles correspond to the right one. The dashed line marks T_N based on the magnetic susceptibility measurements. All data were derived from the neutron powder diffraction refinements.

The magnetic structure has been refined from the neutron powder diffraction patterns at 2 K in a monoclinic unit cell obtained by doubling the nuclear unit cell along the a_m and c_m directions [Fig. 4(b)]. A symmetry analysis based on a
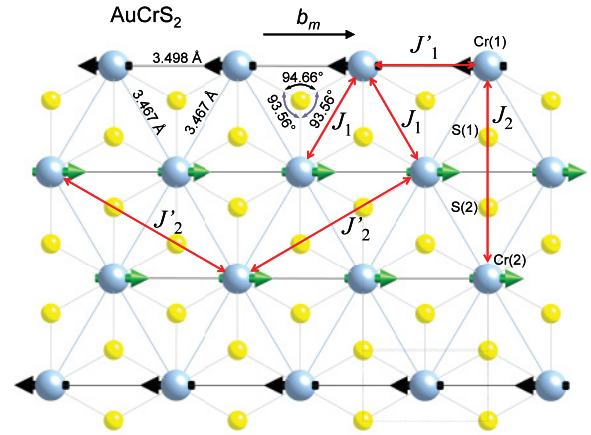

FIG. 6. (Color online) Visualization of the local structure within the Cr plane of AuCrS$_2$ with one underlying and one overlying S layer. Distances and angles are taken from the refinement of the 2 K neutron diffraction data of Table II ($C2/m$ space group). The Cr and S ions are represented by blue and yellow balls, respectively. Full lines correspond to the longer (black) Cr-Cr bonds along b_m and the shorter ones (blue) 120° from b_m. The theoretical intraplane exchange interactions, J_1, J'_1, J_2 and J'_2 are shown as red lines with arrows. Green and black arrows give the direction of the Cr^{3+} magnetic moments, following an up-up-down-down arrangement.

$\mathbf{k} = (\frac{1}{2}\, 0\, \frac{1}{2})$ propagation vector and the $C2/m$ space group gives two possible representations. The first one, Γ_1, corresponds to a magnetic structure described by moments parallel to the [0 1 0] direction. The second representation, Γ_2, has two basis vectors, each corresponding to moments parallel to the [1 0 0] and [0 0 1] directions, respectively. We should adopt the former model Γ_1, which is very similar to that recently proposed for AgCrS$_2$ (Ref. 17), as it accounts better for the intensities of the magnetic peaks at all temperatures. Figure 1(b) shows the good agreement between observed and calculated intensities in the relevant region of the diffraction pattern at 2 K. The refined magnetic structure is commensurate; it consists of double FM chains of Cr^{3+} moments within the hexagonal layers running along b_m. The mutual arrangement of these chains is described by an alternate up-up-down-down sequence both within the Cr planes and along the perpendicular (c_m) direction, as illustrated in Fig. 4(b). This elegant arrangement implies alternate FM and AFM intra- and interplane couplings between adjacent chains, which are stabilized by the residual geometric frustration inherent of the triangular topology. The total moment along [010] has a magnitude of 2.54(4) μ_B at 2 K, which is consistent with the ideal value of 3 μ_B of the $S = 3/2$ Cr^{3+} ion. The slight reduction from the ideal value is expected, considering the covalent properties of the compound. The variation of the magnetic moment with temperature shown in Fig. 3(d) confirms the magnetic ordering temperature of ~47 K, in good agreement with the susceptibility measurements.

IV. DISCUSSION

The specific heat, $C(T)$, curve shows a single sharp peak at T_N, which supports our picture of a simultaneous structural and

magnetic phase transition. The hysteresis obtained upon cooling and warming at low rates confirms the first-order nature of the transition. This conclusion is consistent with the existence of a large spin-lattice coupling, in agreement with previous reports on $NaCrS_2$, $CuCrS_2$, and $AgCrS_2$.[15,17,19] However, the centrosymmetric symmetry of $AuCrS_2$ is incompatible with ferroelectricity, contrary to the latter compound. Thus, the spontaneous polarization observed in monoclinic $AgCrS_2$ is not expected in $AuCrS_2$.

Our observation of simultaneous structural and magnetic phase transition in $AuCrS_2$ gives evidence of a large magnetoelectric coupling. We account for this coupling by noting that the geometric frustration is suppressed by the structural phase transition, thus we infer that the extra elastic energy associated with the structural distortions is overcompensated by the gain of electronic energy associated with the magnetic ordering. The resulting magnetic structure deserves further discussion in light of the complex spin structure observed. We argue that this arrangement arises from a balance between the dominant AFM interaction within the Cr layers and the residual geometric frustration inherent of triangular layers. Under these conditions, both NN and NNN interactions come into play. As to the former ones, the monoclinic distortion results in two different NN interactions; J'_1 along the b_m axis and J_1 along the other two directions at 120° from the b_m axis (Fig. 6). These intralayer couplings between adjacent Cr^{3+} spins can be due either to the direct cation-cation exchange (between two half-filled t_{2g} Cr^{3+} orbitals) or to the indirect superexchange via the Cr-S-Cr path (where the $3p$ orbitals of S are hybridized with the half-filled t_{2g} orbital of one Cr ion and an empty e_g orbital of the other). Taking the Goodenough–Kanamori–Anderson[37,38] rules into consideration, the direct exchange path would be AFM and the superexchange FM as the Cr-S-Cr angle is close to 90°. Direct exchange is more sensitive to the cation-cation distance than the indirect superexchange via the anion. Hence, the former interaction is expected to be predominant for short Cr-Cr distances and the latter for long.

According to Rosenberg et al.,[39] the critical Cr-Cr distance for the occurrence of ferromagnetic superexchange is around 3.6 Å. As the Cr-Cr distances in $AuCrS_2$ are 3.4671(1) Å and 3.4976(1) Å, direct AFM exchange should dominate. Also, the observed negative value of Θ_W indicates predominant antiferromagnetic interactions. However, the observed Cr-Cr distances are very close to the cutoff value ∼3.6 Å proposed by Rosenberg et al., resulting in a competition between the two exchange mechanisms and a weakening of the NN couplings J_1 and J'_1. Also, the geometric frustration involving the NN spins should be taken into account. Therefore, the NNN interactions, J_2 and J'_2, across the Cr-S-S-Cr path are expected to play a decisive role in stabilizing the magnetic structure (Fig. 6). The distortion of the triangular lattice below T_N results in a shortening of the S(1)-S(2) and Cr(1)-Cr(2) distances perpendicular to b_m (J_2), 3.225 Å and 5.988 Å. These values are to be compared with the values of 3.260 and 6.040 Å at 150° to b_m (J'_2). This may increase the strength of the shorter NNN interaction, J_2, as suggested for $CuFeO_2$.[30] In $AuCrS_2$, the exchange, J_2, is AFM on all Cr sites. Hence, the degree of geometric frustration is weakened, leading to the formation of FM spin chains in the b_m direction, where the Cr-Cr distances are larger and an up-up-down-down

arrangement perpendicular to b_m. $CuFeO_2$ also displays the up-up-down-down configuration, but the magnetic coupling along b_m is AFM.

Further studies are required to confirm the above qualitative account of the stability of the collinear magnetic structures observed experimentally. Recent studies on the $CuFeO_2$ system suggest that exchange couplings up to the third-nearest neighbor within the Cr plane should be considered in order to provide a quantitative account of these structures.[40,41]

The magnetic structure of $AuCrS_2$ reported in this paper is in agreement with a neutron inelastic scattering study on $AgCrS_2$ (Ref. 17), which shows that magnetic correlations are significant for NNN interactions involving Cr-Cr distances of 6–7 Å. Indeed, $AgCrS_2$ displays a magnetic structure almost identical to that of $AuCrS_2$. Specifically, the two structures share the following features: (1) the structure consists of FM chains along b_m; (2) the monoclinic distortion leads to two inequivalent NNN distances of 6.0125(2) and 6.0553(1) Å; (3) the magnetic interaction is always antiferromagnetic in the direction of the shorter distance.

Although the interlayer interactions are expected to be weaker than the intralayer ones, they should be taken into account to explain the three-dimensional magnetic structure. In fact, the Cr-Cr interlayer distances are only slightly larger (∼6–7%) than the third NN intralayer ones, and the latter should not be neglected, as mentioned above. The shear distortion of the Cr planes at the monoclinic transition results in two inequivalent interlayer Cr-Cr distances and, hence, in two interlayer exchange couplings, J_3 and J'_3 [see Fig. 4(b)]. In spite of the modest difference between these two distances, it is relevant as the coupling J_3 along the shorter distance is AFM, whereas the coupling J'_3 along the longer distance leads to an up-up-down-down coupling. Note that the same arrangement is found in $AgCrS_2$.[17]

While the magnetic structures of $AuCrS_2$ and $AgCrS_2$ are almost identical, $CuCrS_2$ displays a completely different helical structure.[15] Although, in $CuCrS_2$ as well, the monoclinic distortion results in the formation of two NN Cr bonds, the anisotropy is less pronounced, and the longer Cr-Cr bond is smaller (3.4915 Å) as compared to both $AuCrS_2$ (3.4976 Å) and $AgCrS_2$ (3.5042 Å).[15,17] Therefore, the direct AFM interaction dominates, and the ferromagnetic chains observed in $AuCrS_2$ and $AgCrS_2$ are not present in $CuCrS_2$. This implies that the lattice deformation and the increased Cr-Cr distances are an important factor in the stabilization of the collinear structure of $AuCrS_2$ and $AgCrS_2$. On the other hand, the coordination of the Cr^{3+} ion seems to play a minor role considering that $CuCrS_2$ and $AgCrS_2$ are isostructural but display different magnetic orderings. Our observations are in accordance with the assumption by Engelsman et al.[12] that an increased Cr-Cr distance results in a larger Θ_W indicative of stronger ferromagnetic interactions.

V. CONCLUSIONS

In summary, we have shown that $AuCrS_2$ undergoes a first-order magnetic and structural phase transition at $T_N = 47$ K from a paramagnetic rhombohedral R-$3m$ to a monoclinic antiferromagnetic $C2/m$ symmetry. The simultaneous observation of magnetic and structural transition gives

evidence of a large magnetoelastic coupling. This coupling accounts for the stability of the magnetic order observed, considering that the structural distortions at the transition suppress the geometric frustration of the Cr layers. The peculiar antiferromagnetic structure observed is explained by the interplay between the direct and superexchange interactions involving nearest neighbor and next-nearest neighbor Cr-Cr interactions, as well as the residual frustration in the triangular Cr planes. We envisage that further studies on the stability of the nuclear and magnetic structures may provide a hint to tailor the magnetoelastic coupling and the multiferroic properties in geometrically frustrated sulfides.

*Corresponding author: sandra.karlsson@grenoble.cnrs.fr

[1] T. Kimura, T. Goto, H. Shintani, K. Ishizaka, T. Arima, and Y. Tokura, Nature **426**, 55 (2003).

[2] N. Hur, S. Park, P. A. Sharma, J. S. Ahn, S. Guha, and S. W. Cheong, Nature **429**, 392 (2004).

[3] M. F. Collins and O. A. Petrenko, Can. J. Phys. **75**, 605 (1997).

[4] S. W. Cheong and M. Mostovoy, Nat. Mater. **6**, 13 (2007).

[5] S.-H. Lee, D. Louca, H. Ueda, S. Park, T. J. Sato, M. Isobe, Y. Ueda, S. Rosenkranz, P. Zschack, J. Íñiguez, Y. Qiu, and R. Osborn, Phys. Rev. Lett. **93**, 156407 (2004).

[6] Y. Oohara, S. Mitsuda, H. Yoshizawa, N. Yaguchi, H. Kuriyama, Y. Asana, and M. Mekata, J. Phys. Soc. Jpn. **63**, 847 (1994).

[7] H. Kadowaki, H. Kikuchi, and Y. Ajiro, J. Phys. Condens. Matter **2**, 4485 (1990).

[8] H. Takatsu, H. Yoshizawa, S. Yonezawa, and Y. Maeno, Phys. Rev. B **79**, 104424 (2009).

[9] D. Hsieh, D. Qian, R. F. Berger, R. J. Cava, J. W. Lynn, Q. Huang, and M. Z. Hasan, Physica B **403**, 1341 (2008).

[10] S. Seki, Y. Onose, and Y. Tokura, Phys. Rev. Lett. **101**, 067204 (2008).

[11] K. Kimura, H. Nakamura, K. Ohgushi, and T. Kimura, Phys. Rev. B **78**, 140401(R) (2008).

[12] F. M. R. Engelsman, G. A. Wiegers, F. Jellinek, and B. Van Laar, J. Solid State. Chem. **6**, 574 (1973); B. van Laar and D. J. W. Ijdo, *ibid.* **3**, 590 (1971).

[13] P. F. Bongers, C. F. van Bruggen, J. Koopstra, W. P. F. A. M. Omloo, G. A. Weigers, and F. Jellinek, J. Phys. Chem. Solids **29**, 977 (1968).

[14] M. Wintenberger and Y. Allain, Solid State Commun. **64**, 1343 (1987).

[15] J. C. E. Rasch, M. Boehm, C. Ritter, H. Mutka, J. Schefer, L. Keller, G. M. Abramova, A. Cervellino, and J. F. Löffler, Phys. Rev. B **80**, 104431 (2009).

[16] A. Lafond, W. Henggeler, H. Mutka, and B. Ouaddiaf, Can. J. Phys. **79**, 1427 (2001).

[17] F. Damay, C. Martin, V. Hardy, G. André, S. Petit, and A. Maignan, Phys. Rev. B **83**, 184413 (2011).

[18] K. Singh, A. Maignan, C. Martin, and C. Simon, Chem. Mater. **21**, 5007 (2009).

[19] K. W. Blazey and H. Rohrer, Phys. Rev. **185**, 712 (1969).

[20] H. Fukuoka, S. Sakashita, and S. Yamanaka, J. Solid State Chem. **148**, 487 (1999).

[21] G. Rousse, J. Rodríguez-Carvajal, C. Wurm, and C. Masquelier, Chem. Mater. **13**, 4527 (2001).

[22] G. Rousse, J. Rodríguez-Carvajal, C. Wurm, and C. Masquelier, Solid State Sci. **4**, 973 (2002).

[23] G. Rousse, J. Rodríguez-Carvajal, S. Patoux, and C. Masquelier, Chem. Mater. **15**, 4082 (2003).

[24] B. C. Melot, G. Rousse, J. N. Chotard, M. Ati, J. Rodríguez-Carvajal, M. C. Kemei, J. M. Tarascon, Chem. Mater. **23**, 2922 (2011).

[25] H. M. Rietveld, J. Appl. Crystallogr. **2**, 65 (1969).

[26] A. C. Larson and R. B. Von Dreele, *Los Alamos National Laboratory Report No. LAUR 86-748* (Los Alamos National Laboratory, Los Alamos, NM, 1994).

[27] J. Rodríguez-Carvajal, Physica B **192**, 55 (1993); See [http://www.ill.eu/sites/fullprof/]

[28] E. Nishibori, M. Takata, K. Kato, M. Sakata, Y. Kubota, S. Aoyagi, Y. Kuroiwa, M. Yamakata, and N. Ikeda, Nucl. Instrum. Methods Phys. Res. A **467-468**, 1045 (2001).

[29] J. S. Hwang, K. J. Lin, and C. Tien, Rev. Sci. Instrum. **68**, 94 (1997).

[30] F. Ye, Y. Ren, Q. Huang, J. A. Fernandez-Baca, P. Dau, J. W. Lynn, and T. Kimura, Phys. Rev. B **73**, 220404(R) (2006).

[31] E. Hehle and H. Sabrowsky, Z. Naturforsch. Teil B **30**, 659 (1975).

[32] A. Gauzzi, E. Gilioli, F. Licci, M. Marezio, G. Calestani, C. Franchini, and S. Massidda, Phys. Rev. B **66**, 085106 (2002).

[33] J. E. Greedan, J. Mater. Chem. **11**, 37 (2001).

[34] A. Maignan, C. Martin, R. Frésard, V. Eyert, E. Guilmeau, S. Herbert, M Poienar, and D. Pelloquin, Solid State Comm. **149**, 962 (2009).

[35] H. T. Stokes and D. M. Hatch, "Invariants," *ISOTROPY*, 2002, [http://stokes.byu.edu//invariants.html (01 June 2011)].

[36] L. Landau and E. Lifshitz, *Statistical Physics* (Pergamon, New York, 1980).

[37] J. B. Goodenough, *Magnetism and the Chemical Bond* (Interscience, New York, 1963).

[38] J. Kanamori, J. Phys. Chem. Solids **10**, 87 (1959).

[39] M. Rosenberg, A. Knülle, H. Sabrowsky, and C. Platte, J. Phys. Chem. Solids **43**, 574 (1982).

[40] M. Mekata, N. Yagushi, T. Takagi, T. Sugino, S. Mitsuda, H. Yoshizawa, N. Hosoito, and T. Shinjo, J. Phys. Soc. Jpn. **62**, 4474 (1993).

[41] S. Mitsuda, N. Kasahara, T. Uno, and M. Mase, J. Phys. Soc. Jpn. **67**, 4026 (1998).